Robust Control Design for the Poloidal Magnetic Flux Profile Evolution in the Presence of Model Uncertainties

Yongsheng Ou, Chao Xu, and Eugenio Schuster

***Abstract*—The potential operation of a tokamak fusion reactor in a highly efficient steady-state mode is directly related to the achievement of certain types of radial profiles for the current flowing toroidally in the device. The evolution in time of the toroidal current profile in tokamaks is related to the evolution of the poloidal magnetic flux profile, which is modeled in normalized cylindrical coordinates using a nonlinear partial differential equation usually referred to as the magnetic diffusion equation. We propose a robust control scheme to regulate the poloidal magnetic flux profile in tokamaks in the presence of model uncertainties. These uncertainties come mainly from the resistivity term of the magnetic diffusion equation. First, we either simulate the magnetic diffusion equation or carry out experiments to generate data ensembles, from which we then extract the most energetic modes to obtain a reduced-order model based on proper orthogonal decomposition and Galerkin projection. The obtained reduced-order model corresponds to a linear state-space representation with uncertainty. Taking advantage of the structure of the state matrices, the reduced-order model is reformulated into a robust control framework, with the resistivity term as an uncertain parameter. An H_∞ controller is designed to minimize the regulation/tracking error. Finally, the synthesized model-based robust controller is tested in simulations.**

***Index Terms*—Current profile control, distributed parameter systems, POD, robust control, tokamak plasma control.**

I. Introduction

SETTING UP a suitable current profile, which is proportional to the spatial derivative of the poloidal flux profile, has been demonstrated to be a key condition for one possible advanced scenario with improved confinement and possible steady-state operation [1]. One approach to current-profile control is to focus on creating the desired current profile during the plasma-current ramp-up and early flat-top phases (finite-time optimal control problem) with the aim of maintaining this target profile during the subsequent phases of the discharge (regulation problem).

Our previous work includes the investigation of the use of extremum seeking (ES) [2] and nonlinear programming [3] to achieve open-loop solutions for the optimal control problem defined during the ramp-up and early flat-top phases. The time evolutions of the control inputs are obtained in the interval $[0, T]$ in order to minimize the quadratic error between the actual and desired current profiles at time T (see Fig. 1). This paper is aimed at saving long trial-and-error periods of time currently spent by fusion experimentalists trying to manually adjust the time evolutions of the actuators to achieve the desired current profile at some time T within a prespecified window $[T_1, T_2]$.

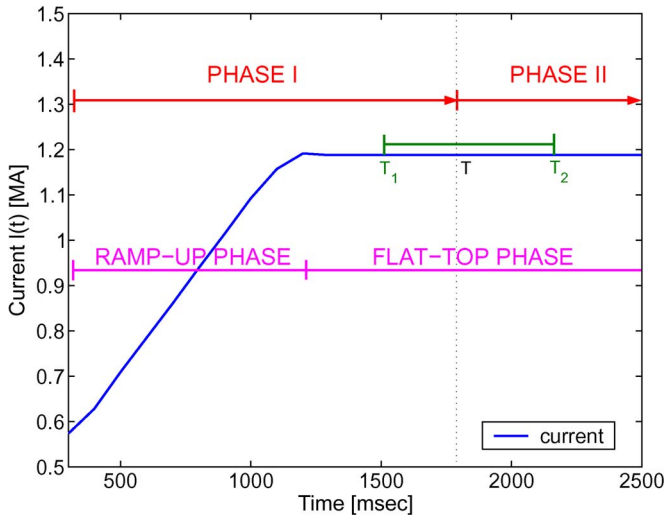

Fig. 1. Total plasma-current evolution can be roughly divided into two phases, which are the ramp-up and flat-top phases. During Phase I (ramp-up phase and the first part of the flat-top phase), the control goal is to drive the magnetic flux profile from some initial arbitrary condition to a predefined target profile at some time T between the time window $[T_1, T_2]$, which is in the flat-top phase.

These open-loop solutions depend on the plasma resistivity, and therefore on the electron temperature, whose dynamics is very difficult to be predicted by simple control-oriented models [4]. In this paper, we take into account the unmodeled temperature dynamics by considering the resistivity coefficient in the magnetic diffusion equation as an uncertainty. After reducing the dimensionality of the magnetic diffusion equation by combining proper orthogonal decomposition (POD) and Galerkin projection [5], the model for the poloidal flux is written within a robust control framework. A robust controller minimizing the H_∞ norm of the sensitivity function of the closed-loop system is then designed to reduce the tracking/regulation error.

This paper is organized as follows. The dynamic model for the poloidal flux is introduced in Section II. The model reduction technique is explained in Section III. Section IV

Manuscript received July 13, 2009; revised November 18, 2009. First published February 2, 2010; current version published March 10, 2010. This work was supported by the NSF CAREER Award under Program ECCS-0645086.

The authors are with the Department of Mechanical Engineering and Mechanics, Lehigh University, Bethlehem, PA 18015 USA (e-mail: yoo205@lehigh.edu).

Color versions of one or more of the figures in this paper are available online at http://ieeexplore.ieee.org.

Digital Object Identifier 10.1109/TPS.2009.2038476

describes how the model is written within a robust control framework. The controller is designed and tested in simulations in Section V. This paper is closed with the conclusions in Section VI.

II. Current-Profile Evolution Model

Let ρ be an arbitrary coordinate indexing the magnetic surface. Any quantity constant on each magnetic surface could be chosen as the variable ρ. We choose the mean geometric radius [6] of the magnetic surface as the variable ρ, i.e., $\pi B_{\phi,o}\rho^2 = \Phi$, where Φ is the toroidal magnetic flux and $B_{\phi,o}$ is the reference toroidal magnetic field at the geometric plasma center R_o. The variable $\hat{\rho}$ denotes the normalized radius (ρ/ρ_b), and ρ_b is the radius of the last closed flux surface. The evolution of the poloidal flux in normalized cylindrical coordinates is given by the magnetic diffusion equation [7]

$$\frac{\partial \psi}{\partial t} = \frac{\eta(T_e)}{\mu_o \rho_b^2 \hat{F}^2 \hat{\rho}} \frac{\partial}{\partial \hat{\rho}} \left(\hat{\rho} \hat{F} \hat{G} \hat{H} \frac{\partial \psi}{\partial \hat{\rho}} \right) - R_o \hat{H} \eta(T_e) \frac{\langle \bar{j}_{NI} \cdot \bar{B} \rangle}{B_{\phi,o}} \tag{1}$$

where t is the time, ψ is the poloidal magnetic flux, η is the plasma resistivity, T_e is the plasma electron temperature, $\mu_o = 4\pi \times 10^{-7}$ (H/m) is the vacuum permeability, $\bar{j}_{\mathrm{NI}}$ is the noninductive source of current density (neutral beam, electron cyclotron, etc.), $\overline{B}$ is the magnetic field, and $\langle\rangle$ denotes flux-surface average. $\hat{F}$, $\hat{G}$, and $\hat{H}$ are geometric factors, which are functions of $\hat{\rho}$. The boundary conditions are given by

$$\left.\frac{\partial \psi}{\partial \hat{\rho}}\right|_{\hat{\rho}=0} = 0 \qquad \left.\frac{\partial \psi}{\partial \hat{\rho}}\right|_{\hat{\rho}=1} = \frac{\mu_o}{2\pi} \frac{R_o}{\hat{G}\Big|_{\hat{\rho}=1} \hat{H}\Big|_{\hat{\rho}=1}} I(t) \tag{2}$$

where $I(t)$ denotes the total toroidal plasma current.

The current density that flows toroidally around the tokamak $\langle \bar{j} \cdot \overline{B}/B_{\phi,o} \rangle$ and whose profile must be controlled is related to the spatial derivative of the poloidal magnetic flux

$$\frac{\langle \bar{j} \cdot \bar{B} \rangle}{B_{\phi,o}} = \frac{1}{\mu_o \rho_b^2 \hat{F}^2 \hat{H} \hat{\rho}} \frac{\partial}{\partial \hat{\rho}} \left(\hat{\rho} \hat{F} \hat{G} \hat{H} \frac{1}{R_0} \frac{\partial \psi}{\partial \hat{\rho}} \right). \tag{3}$$

The model makes the simplifying assumption that the magnetic geometry is fixed in time. This excludes two potential sources of flux—a change in ρ_b (either by a change in the shape of the last closed flux surface or in $B_{\phi,o}$) and a change in the location of the geometric center of the interior flux surfaces relative to that of the last closed flux surface. Changes in ρ_b are small by design in the experiments of interest, but it is straightforward to include this effect in the model for situations where it would be important. Changes in the relative positions of the flux surfaces do occur, but for cases of interest, these happen slowly enough and they can be neglected.

A simplified scenario-oriented model for the noninductive toroidal current density is chosen for Phase I (see Fig. 1). Based on experimental observations at DIII-D, the shape of the profile is assumed to remain fixed and equal to the so-called reference profile $j_{\mathrm{NIpar}}^{\mathrm{profile}}(\hat{\rho})$, which is identified from DIII-D discharges associated with the experiment of interest and shown in Fig. 2 [7]. The response to the actuators is simply a scalar multiple of

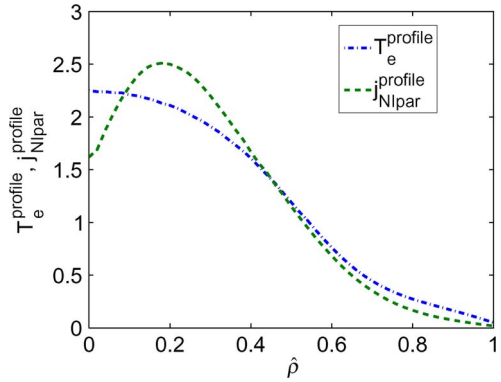

Fig. 2. Temperature $(T_e^{\mathrm{profile}}(\hat{\rho}))$ and noninductive toroidal current density $(j_{\mathrm{NIpar}}^{\mathrm{profile}}(\hat{\rho}))$ profiles.

the reference profile. The noninductive toroidal current density $(\langle \bar{j}_{\mathrm{NI}} \cdot \overline{B} \rangle / B_{\phi,o})$ is assumed to follow

$$\frac{\langle \bar{j}_{NI} \cdot \bar{B} \rangle}{B_{\phi,o}} = k_{\mathrm{NIpar}} j_{\mathrm{NIpar}}^{\mathrm{profile}}(\hat{\rho}) \frac{I(t)^{1/2} P_{\mathrm{tot}}(t)^{5/4}}{\bar{n}(t)^{3/2}} \tag{4}$$

where $k_{\mathrm{NIpar}} = 1.2139 \cdot 10^{18}$ $(\mathrm{m}^{-9/2} \cdot \mathrm{A}^{-1/2} \cdot \mathrm{W}^{-5/4})$ and P_{tot} is the total power of the noninductive current sources (electron cyclotron heating, neutral beam heating, etc.). The line-averaged plasma density is denoted by $\overline{n}$.

The resistivity η scales with the temperature T_e as

$$\eta(\hat{\rho}, t) = \frac{k_{\mathrm{eff}} Z_{\mathrm{eff}}}{T_e^{3/2}(\hat{\rho}, t)} \tag{5}$$

where $Z_{\mathrm{eff}} = 1.5$ and $k_{\mathrm{eff}} = 4.2702 \cdot 10^{-8}$ $(\Omega \cdot \mathrm{m}(\mathrm{keV})^{3/2})$.

It is worth noting that we can rewrite the equation for the evolution of the poloidal flux (1) as

$$\frac{\partial \psi}{\partial t} \nu(\hat{\rho}, t) \frac{1}{\hat{\rho}} \frac{\partial}{\partial \hat{\rho}} \left(\hat{\rho} f_4(\hat{\rho}) \frac{\partial \psi}{\partial \hat{\rho}} \right) + \nu(\hat{\rho}, t) f_2(\hat{\rho}) u_1(t) \tag{6}$$

with boundary conditions

$$\left.\frac{\partial \psi}{\partial \hat{\rho}}\right|_{\hat{\rho}=0} = 0 \qquad \left.\frac{\partial \psi}{\partial \hat{\rho}}\right|_{\hat{\rho}=1} = u_2(t) \tag{7}$$

initial condition $\psi_0(\hat{\rho}) = \psi(\hat{\rho}, 0)$, and

$$\nu(\hat{\rho}, t) = \frac{\eta(T_e)}{\mu_o \rho_b^2 \hat{F}^2} \tag{8}$$

$$f_2(\hat{\rho}) = -R_o \hat{H} \mu_o \rho_b^2 \hat{F}^2(\hat{\rho}) k_{\mathrm{NIpar}} j_{\mathrm{NIpar}}^{\mathrm{profile}}(\hat{\rho}) \tag{9}$$

$$u_1(t) = \frac{I(t)^{1/2} P_{\mathrm{tot}}(t)^{5/4}}{\bar{n}(t)^{3/2}} \tag{10}$$

$$u_2(t) = k_3 I(t), \qquad k_3 = \frac{\mu_o}{2\pi} \frac{R_o}{\hat{G}\Big|_{\hat{\rho}=1} \hat{H}\Big|_{\hat{\rho}=1}} \tag{11}$$

$$f_4(\hat{\rho}) = \hat{F} \hat{G} \hat{H}. \tag{12}$$

In practice, it is very difficult to accurately predict the time evolution of the electron temperature T_e, and consequently of the plasma resistivity $\eta(T_e)$, by a model that is simple enough for control design. Therefore, in this paper, we integrate

$\eta(T_e)$ into $\nu(\hat{\rho},t)$ and model it as an uncertainty as explained hereafter.

III. Model Reduction Using POD/Galerkin

A. POD Modes

First, we either simulate the magnetic diffusion equation (1) on the grid $\mathcal{Q}_{ij}=(\hat{\rho}_i,t_j)$, where i and j are integers with $1\leq i\leq\overline{m}$ and $1\leq j\leq\overline{n}$, respectively, or carry out experiments to generate data ensembles from which the most energetic modes can be extracted. The set $\mathcal{V}=\text{span}\{\psi_1,\ldots,\psi_{\overline{n}}\}\subset\mathbb{R}^{\overline{m}}$ refers to a data ensemble consisting of snapshots $\{\psi_j\}_{j=1}^{\overline{n}}$ obtained at $\overline{n}$ different instants of time either from simulations or experiments. The goal of the POD method is to find an orthonormal basis $\{\phi_k\}_{k=1}^{l}$ such that, for some predefined $1\leq l\leq d$, where $d=\dim\mathcal{V}\leq\overline{m}$, the reconstruction error for the snapshots is minimized, i.e.,

$$\min_{\{\phi_k\}_{k=1}^{l}}\frac{1}{\overline{n}}\sum_{j=1}^{\bar{n}}\left\|\psi_j-\sum_{k=1}^{l}(\psi_j,\phi_k)\phi_k\right\|^2 \tag{13}$$

subject to

$$(\phi_i,\phi_j)=\delta_{ij},\qquad 1\leq i\leq l;1\leq j\leq i$$

where $\|\psi\|=\sqrt{\psi^{\mathrm{T}}\psi}$ and $(\cdot,\cdot)$ denotes the inner product in the space $L^2([0,1])$.

Let $\Lambda_1>\cdots>\Lambda_l>\cdots>\Lambda_d>0$ denote the positive eigenvalues of the correlation matrix $\overline{K}$, defined as $\overline{K}_{ij}=(1/\overline{n})(\psi_j,\psi_i)$, for $i,j=1,\ldots,\overline{n}$, and $v_1,\ldots,v_l,\ldots,v_d$ denote the associated unit-norm eigenvectors, where $d=\text{rank}(K)$. Then, the POD basis functions take the form [5]

$$\phi_k=\frac{1}{\sqrt{\Lambda_k}}\sum_{j=1}^{\bar{n}}(v_k)_j\psi_j=\frac{1}{\sqrt{\Lambda_k}}Yv_k,\qquad k=1,\ldots,d \tag{14}$$

where $(v_k)_j$ is the jth component of the eigenvector v_k and $Y=(\psi_1,\ldots,\psi_n)$ is the collection of all the snapshots. Moreover, the error (energy ratio) associated with the approximation with the first l POD modes is

$$\varepsilon_l=\frac{1}{\overline{n}}\sum_{j=1}^{\bar{n}}\left\|\psi_j-\sum_{k=1}^{l}\left(\psi_j^{\mathrm{T}}\phi_k\right)\phi_k\right\|^2=\sum_{k=l+1}^{d}\Lambda_k. \tag{15}$$

B. Galerkin Projection

Let $V=\{z|z,(\mathrm{d}z/\mathrm{d}\hat{\rho})\in L^2(\hat{\rho})\}$ and $\phi(\hat{\rho})\in V$ be a test function, where $\hat{\rho}\in[0,1]$. Let $V_{\text{POD}}=\text{span}\{\phi_1,\phi_2,\phi_3,\phi_4,\ldots,\phi_l\}\subset V$ be a space spanned by the POD modes obtained from the model reduction process for $\psi(\hat{\rho},t)$. Let

$$\psi(\hat{\rho},t)\approx\psi^l(\hat{\rho},t)=\sum_{k=1}^{l}\beta_k(t)\phi_k(\hat{\rho}) \tag{16}$$

where $\phi_k(\hat{\rho})\in V_{\text{POD}}$, $k=1,2,\ldots,l$. Similarly, let $W_{\text{POD}}=\text{span}\{\varphi_1,\varphi_2,\varphi_3,\varphi_4,\ldots,\varphi_n\}\subset W$ be a space spanned by the POD modes obtained from the model reduction process for $\nu(\hat{\rho},t)$. We write

$$\nu(\hat{\rho},t)\approx\nu^n(\hat{\rho},t)=\sum_{i=1}^{n}\gamma_i(t)\varphi_i(\hat{\rho}) \tag{17}$$

where $\Gamma=(\gamma_1,\ldots,\gamma_n)^{\mathrm{T}}\in\mathbb{R}^n$ is the uncertainty vector and $\varphi_i(\hat{\rho})\in W_{\text{POD}}$, $i=1,2,\ldots,n$. The vector Γ is the finite dimensional approximation of $\nu(\hat{\rho},t)$ with respect to the obtained POD modes. Each element γ_i of Γ is a time-varying uncertainty associated with $\varphi_i(\hat{\rho})$, which is modeled as $\gamma_i=\gamma_i^0(1+\delta_i)$ with $|\delta_i|<1$ for all i.

We rewrite (6) in its *weak form* by multiplying both sides by $\hat{\rho}\phi(\hat{\rho})$ and integrating over the spatial domain [0, 1], i.e.,

$$\int_0^1\hat{\rho}\phi(\hat{\rho})\frac{\partial\psi(\hat{\rho},t)}{\partial t}\,\mathrm{d}\hat{\rho}=\int_0^1\phi(\hat{\rho})\nu(\hat{\rho})\frac{\partial}{\partial\hat{\rho}}\left(\hat{\rho}f_4(\hat{\rho})\frac{\partial\psi(\hat{\rho},t)}{\partial\hat{\rho}}\right)\mathrm{d}\hat{\rho}+\int_0^1\hat{\rho}\phi(\hat{\rho})f_2(\hat{\rho})\nu(\hat{\rho})u_1(t)\,\mathrm{d}\hat{\rho}. \tag{18}$$

We integrate by parts the second part of (18), taking into account the boundary conditions, to finally obtain

$$\begin{aligned}\frac{\partial}{\partial t}&\int_0^1\hat{\rho}\phi(\hat{\rho})\psi(\hat{\rho},t)\,\mathrm{d}\hat{\rho}\\&=u_2(t)\phi(1)\nu(1)f_4(1)+u_1(t)\int_0^1\hat{\rho}\phi(\hat{\rho})\nu(\hat{\rho})f_2(\hat{\rho})\,\mathrm{d}\hat{\rho}\\&\quad-\int_0^1 f_4(\hat{\rho})(\phi'(\hat{\rho})\nu(\hat{\rho})+\phi(\hat{\rho})\nu'(\hat{\rho}))\,\psi'(\hat{\rho},t)\hat{\rho}\,\mathrm{d}\hat{\rho}\end{aligned}$$

where $F'=\partial F/\partial\hat{\rho}$.

Taking into account (16) and (17) and using the notation

$$\langle\langle g_1,g_2,\ldots g_n\rangle\rangle\triangleq\int_0^1 g_1(\hat{\rho})g_2(\hat{\rho})\cdots g_n(\hat{\rho})\hat{\rho}\,\mathrm{d}\hat{\rho} \tag{19}$$

and

$$\begin{aligned}M_{jk}&=\langle\langle\phi_k,\phi_j\rangle\rangle\\K_{jk}&=\sum_{i=1}^{n}\gamma_i\left(\left\langle\left\langle f_4\phi_k',\phi_j',\varphi_i\right\rangle\right\rangle+\langle\langle f_4\phi_k',\phi_j,\varphi_i'\rangle\rangle\right)\\P_j&=\sum_{i=1}^{n}\gamma_i\langle\langle\phi_j,f_2,\varphi_i\rangle\rangle\\Q_j&=\sum_{i=1}^{n}\gamma_i f_4(1)k_3\phi_j(1)\varphi_i(1)\end{aligned} \tag{20}$$

we obtain a matrix representation for the reduced-order model

$$M\frac{\mathrm{d}x}{\mathrm{d}t}=-Kx+Pu_1+Qu_2 \tag{21}$$

where $x(t)=(\beta_1,\ldots,\beta_l)^{\mathrm{T}}\in\mathbb{R}^l$, $M,K\in\mathbb{R}^{l\times l}$, and $P,Q\in\mathbb{R}^l$. The vector $x(t)$ is the finite dimensional approximation of

$\psi(\hat{\rho}, t)$ with respect to the obtained POD modes. The components of the initial state are given by

$$x^i(t_0) = x_0^i = (\psi(t_0), \phi_i), \qquad i = 1, \ldots, l \tag{22}$$

where $x_0 \in \mathbb{R}^{l\times 1}$ and ϕ_i, for $i = 1, \ldots, l$, denotes the POD modes.

Since M is invertible by the definition of the POD modes, the state-space representation of the reduced-order model is written as

$$\begin{cases} \dot{x} = Ax + Bu \\ y = Cx + Du \end{cases} \tag{23}$$

where $A = -M^{-1}K \in \mathbb{R}^{l\times l}$, $B = M^{-1}[P\, Q] \in \mathbb{R}^{l\times 2}$, $C = I_l$ is an $l \times l$ identity matrix, $D = 0$, and $u(t) = [u_1(t)\, u_2(t)]^{\mathrm{T}}$.

We let $u^o(t) = [u_1^o\ u_2^o]^{\mathrm{T}}$ be a set of open-loop control trajectories, which are computed offline, and $x^o(t)$ be the open-loop state trajectory associated to the open-loop control $u^o(t)$, with a nominal initial state x_0^o. The open-loop state trajectory satisfies

$$M\frac{\mathrm{d}x^o}{\mathrm{d}t} = -Kx^o + Pu_1^o + Qu_2^o \tag{24}$$

with initial condition $x^o(t_0) = x_0^o$.

Let us define

$$e(t) = x(t) - x^o(t) \quad u^c(t) = u(t) - u^o(t) \tag{25}$$

where $u(t)$ is the total control input and $u^c(t) = [u_1^c\ u_2^c]^{\mathrm{T}}$ is the to-be-designed closed-loop control, which is appended to the open-loop control $u^o(t)$. Then, we can write

$$\frac{\mathrm{d}e}{\mathrm{d}t} = Ae + Bu^c + d \tag{26}$$

where $d(t) = -M^{-1}(K - K^o)x^o(t) + M^{-1}(P - P^o)u_1^o(t) + M^{-1}(Q - Q^o)u_2^o(t)$. In this paper, we assume that $x(t)$, and therefore $e(t)$, is measurable.

IV. Model in Robust Control Framework

A system with state-space representations A, B, C, and D has a transfer function $G(s) = D + C(sI_l - A^{-1})B$, where l is the number of states in the system. Defining the matrix

$$M_a = \begin{bmatrix} A & B \\ C & D \end{bmatrix} \tag{27}$$

we can write the transfer function as a linear fractional transformation (LFT)

$$\begin{aligned} G(s) &= F_u\left(M_a, \frac{1}{s}I_l\right) \\ &= M_{a_{22}} + M_{a_{21}}\frac{1}{s}I_l\left(I_l - M_{a_{11}}\frac{1}{s}I_l\right)^{-1}M_{a_{12}} \\ &= D + C\frac{1}{s}I_l\left(I_l - A\frac{1}{s}I_l\right)^{-1}B \\ &= D + C(sI_l - A^{-1})B. \end{aligned} \tag{28}$$

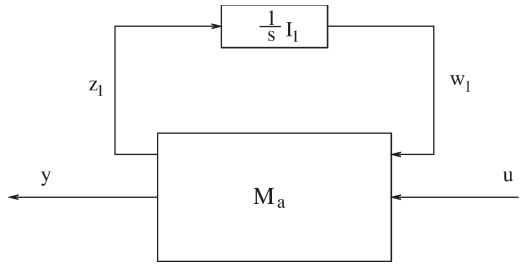

Fig. 3. $G(s)$ as an LFT using M_a, $(1/s)I_l$.

The graphical representation of $G(s)$ is shown in Fig. 3 with equivalent equations

$$\begin{bmatrix} z_1 \\ y \end{bmatrix} = \begin{bmatrix} A & B \\ C & D \end{bmatrix}\begin{bmatrix} w_1 \\ u \end{bmatrix}$$
$$w_1 = \frac{1}{s}z_1; y = F_u\left(M_a, \frac{1}{s}I_l\right)u = G(s)u. \tag{29}$$

To make the uncertainty in the state-space system (23) explicit, the matrices K, P, and Q can be rewritten as

$$K = \hat{K}_0 + \sum_{i=1}^{n}\delta_i\hat{K}_i \quad P = \hat{P}_0 + \sum_{i=1}^{n}\delta_i\hat{P}_i \quad Q = \hat{Q}_0 + \sum_{i=1}^{n}\delta_i\hat{Q}_i \tag{30}$$

where

$$\hat{K}_{0_{jk}} = \sum_{i=1}^{n}\gamma_i^0\left(\langle f_4\phi_k', \phi_j', \varphi_i\rangle + \langle f_4\phi_k', \phi_j, \varphi_i'\rangle\right) \tag{31}$$

$$\hat{K}_{i_{jk}} = \gamma_i^0\left(\langle f_4\phi_k', \phi_j', \varphi_i\rangle + \langle f_4\phi_k', \phi_j, \varphi_i'\rangle\right) \tag{32}$$

$$\hat{P}_{0_j} = \sum_{i=1}^{n}\gamma_i^0\langle\phi_j, f_2, \varphi_i\rangle \tag{33}$$

$$\hat{P}_{i_j} = \gamma_i^0\langle\phi_j, f_2, \varphi_i\rangle \tag{34}$$

$$\hat{Q}_{0_j} = \sum_{i=1}^{n}\gamma_i^0 f_4(1)k_3\phi_j(1)\varphi_i(1) \tag{35}$$

$$\hat{Q}_{i_j} = \gamma_i^0 f_4(1)k_3\phi_j(1)\varphi_i(1). \tag{36}$$

Then, we define the matrix M_a as a general affine state-space uncertainty

$$M_a = \begin{bmatrix} A_0 + \sum_{i=1}^{n}\delta_i A_i B_0 + \sum_{i=1}^{n}\delta_i B_i \\ C_0 + \sum_{i=1}^{n}\delta_i C_i D_0 + \sum_{i=1}^{n}\delta_i D_i \end{bmatrix} \tag{37}$$

with $A_0 = -M^{-1}\hat{K}_0 \in \mathbb{R}^{l\times l}$, $A_i = -M^{-1}\hat{K}_i \in \mathbb{R}^{l\times l}$, $B_0 = M^{-1}[\hat{P}_0\ \hat{Q}_0] \in \mathbb{R}^{l\times 2}$, $B_i = M^{-1}[\hat{P}_i\ \hat{Q}_i]$, $C_0 = I_l$, $C_i = 0$, and $D_0 = D_i = 0$ for all $i = 1, 2, \ldots, n$.

This uncertainty can be formulated into an LFT by achieving the smallest number of repeated blocks using the method outlined in [8]. With this purpose, the matrix J_i is formed as

$$J_i = \begin{bmatrix} A_i & B_i \\ C_i & D_i \end{bmatrix} \in \mathbb{R}^{2l\times(l+2)}. \tag{38}$$

Using singular-value decomposition and grouping terms, the matrix J_i can be expressed as

$$J_i = U_i \Sigma_i V_i^* = (U_i \sqrt{\Sigma}) \left(\sqrt{\Sigma} V_i^* \right) = \begin{bmatrix} L_i \\ W_i \end{bmatrix} \begin{bmatrix} R_i \\ Z_i \end{bmatrix}^* \quad (39)$$

where A^* denotes the complex conjugate transpose of A. By denoting q_i as the rank of matrix J_i, each inner matrix is given by

$$L_i \in \mathbb{R}^{l \times q_i} \quad W_i \in \mathbb{R}^{l \times q_i} \quad R_i \in \mathbb{R}^{l \times q_i} \quad Z_i \in \mathbb{R}^{2 \times q_i}.$$

Then, the uncertainty can be written as

$$\delta_i J_i = \begin{bmatrix} L_i \\ W_i \end{bmatrix} [\delta_i I_{q_i}] \begin{bmatrix} R_i \\ Z_i \end{bmatrix}^* \quad (40)$$

where $q_i = l$ for all $i = 1, 2, \ldots, n$ in this case ($C_i = D_i = 0$). Therefore, the matrix M_a can be written as

$$M_a = M_{11} + M_{12} \Delta M_{21} \quad (41)$$

where

$$M_{11} = \begin{bmatrix} A_0 & B_0 \\ C_0 & D_0 \end{bmatrix} \quad M_{12} = \begin{bmatrix} L_1 & \cdots & L_n \\ W_1 & \cdots & W_n \end{bmatrix}$$
$$M_{21} = \begin{bmatrix} R_1^* & Z_1^* \\ \vdots & \vdots \\ R_n^* & Z_n^* \end{bmatrix} \quad \Delta = \begin{bmatrix} \delta_1 I_{q_1} & & 0 \\ & \ddots & \\ 0 & & \delta_n I_{q_n} \end{bmatrix}.$$

This is equal to the lower LFT

$$\begin{aligned} M_a &= F_l(M, \Delta) \\ &= M_{11} + M_{12} \Delta (I_{q_T} - M_{22} \Delta)^{-1} M_{21} \\ &= M_{11} + M_{12} \Delta M_{21} \end{aligned} \quad (42)$$

where

$$M = \begin{bmatrix} M_{11} & M_{12} \\ M_{21} & 0 \end{bmatrix}$$

and q_T is the total rank of the Δ matrix given by

$$q_T = \sum_i^n q_i = ln.$$

Finally, the transfer function $G(s)$ of the uncertain state-space model is written as

$$G(s) = F_u \left(M_a, \frac{1}{s} I_l \right) = F_u \left(F_l \left(\begin{bmatrix} M_{11} & M_{12} \\ M_{21} & 0 \end{bmatrix}, \Delta \right), \frac{1}{s} I_l \right).$$

The graphical representation of $G(s)$ is shown in Fig. 4 with equivalent equations

$$\begin{bmatrix} \begin{bmatrix} z_1 \\ y \\ z_2 \end{bmatrix} \end{bmatrix} = \begin{bmatrix} M_{11} & M_{12} \\ M_{21} & 0 \end{bmatrix} \begin{bmatrix} \begin{bmatrix} w_1 \\ u \\ w_2 \end{bmatrix} \end{bmatrix}$$
$$w_1 = \frac{1}{s} z_1; w_2 = \Delta z_2;$$
$$y = F_u \left(F_l(M, \Delta), \frac{1}{s} I_l \right) u = G(s) u.$$

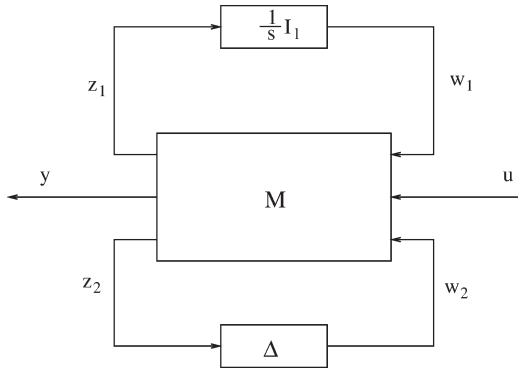

Fig. 4. $G(s)$ as an LFT using M, $\Delta(1/s)I_l$.

The system given by $F_u(F_l(M, \triangle), (1/s)I_l)$ can be written as

$$\begin{aligned} G(s) &= F_u \left(F_l(M, \triangle), \frac{1}{s} I_l \right) = F_l \left(F_u(M, \frac{1}{s} I_l), \triangle \right) \\ &= F_l(P', \triangle) \end{aligned} \quad (43)$$

where $P' = F_u(M, (1/s)I_l)$. The next step in the system reduction moves the uncertainty, creating an upper LFT for convention purposes. This is performed by using

$$G(s) = F_l(P', \triangle) = F_u(P, \triangle)$$

where P' is of the form

$$P' = \begin{bmatrix} P'_{11} & P'_{12} \\ P'_{21} & P'_{22} \end{bmatrix} \quad P = \begin{bmatrix} P'_{22} & P'_{21} \\ P'_{12} & P'_{11} \end{bmatrix}.$$

The overall system reduction is shown in Fig. 5.

The goal is to design a controller that can robustly track the optimal open-loop trajectories of magnetic flux ψ and meet special performance requirements. Therefore, let us consider the reference r and disturbance d as inputs and a weighted version of the tracking error as the output $z = W_p e$, where W_p is a weight chosen by the designer. The overall feedback system is shown in Fig. 6.

We rewrite the plant in the general $\triangle - P - K$ configuration (shown in Fig. 6) in order to enable tracking. Considering $w_2 = u_\Delta$ and $z_2 = y_\Delta$, we get the following equations for the inputs and outputs of p:

$$\begin{aligned} y_\Delta &= P_{11} u_\Delta + P_{12} u \\ y &= P_{21} u_\Delta + P_{22} u \end{aligned}$$

where $P_{11} \in \mathbb{R}^{q_T \times q_T}$, $P_{12} \in \mathbb{R}^{q_T \times 2}$, $P_{21} \in \mathbb{R}^{l \times q_T}$, and $P_{22} \in \mathbb{R}^{l \times 2}$, so that the plant P from $[u_\Delta \; u]^{\mathrm{T}}$ to $[y_\Delta \; y]^{\mathrm{T}}$ is

$$P = \left[\begin{array}{c|c} P_{11} & P_{12} \\ \hline P_{21} & P_{22} \end{array} \right].$$

The diagram in Fig. 7 shows the rewritten feedback system. From the diagram, we obtain the relationship between the inputs and outputs

$$\begin{aligned} y_\Delta &= P_{11} u_\Delta + P_{12} u \\ z &= W_P(-d - P_{21} u_\Delta - P_{22} u + r) \\ e &= -d - P_{21} u_\Delta - P_{22} u + r \end{aligned}$$

where $e \in \mathbb{R}^{l \times 1}$, $d \in \mathbb{R}^{l \times 1}$, and $r \in \mathbb{R}^{l \times 1}$.

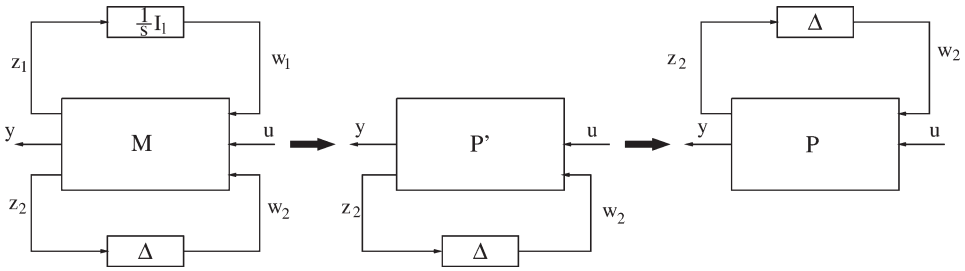

Fig. 5. Diagram of $G(s)$ manipulation.

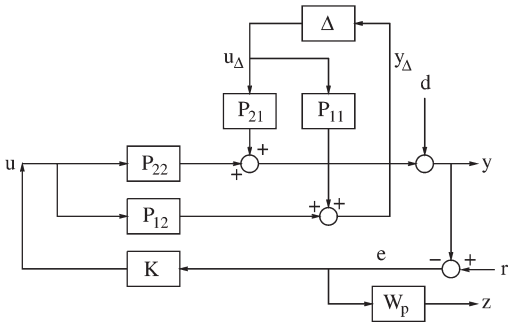

Fig. 6. Overall feedback system.

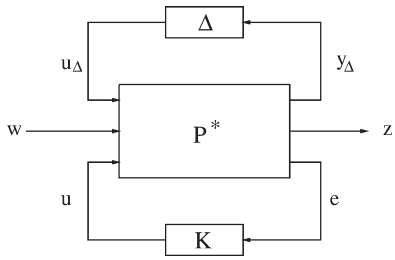

Fig. 7. Robust control framework for augmented plant P^*.

Then, the generalized plan P^* from $[u_\Delta \quad d \quad r \quad u]^{\mathrm{T}}$ to $[y_\Delta \quad z \quad e]^{\mathrm{T}}$ can be written as (see Fig. 7)

$$P^* = \begin{bmatrix} P_{11} & 0 & 0 & P_{12} \\ -W_P P_{21} & -W_P & W_P & -W_P P_{22} \\ -P_{21} & -1 & 1 & P_{22} \end{bmatrix}.$$

V. Controller Synthesis and Simulations

Let us consider the tracking error dynamics given by (26). The control objective is to keep the tracking error e small and to reduce the effect of the disturbance d simultaneously. In our system (see Fig. 6), the tracking error e is governed by

$$e = r - y = \underbrace{(I + KG)^{-1}}_{S}(r - d). \tag{44}$$

In (44), we recognize the sensitivity transfer function S relating the tracking error to both the disturbance d and the reference signal r. Therefore, we have to keep S small at least in both the disturbance and the reference frequency bandwidths. The optimization problem is to find an H_∞ controller K to minimize $\|W_p S\|_\infty$, where $S = (1 + KG)^{-1}$ and the weight function W_p is defined as

$$W_P = \frac{\left(s/M_P^{1/2} + \omega_B^*\right)^2}{\left(s + \omega_B^* A^{*1/2}\right)^2}. \tag{45}$$

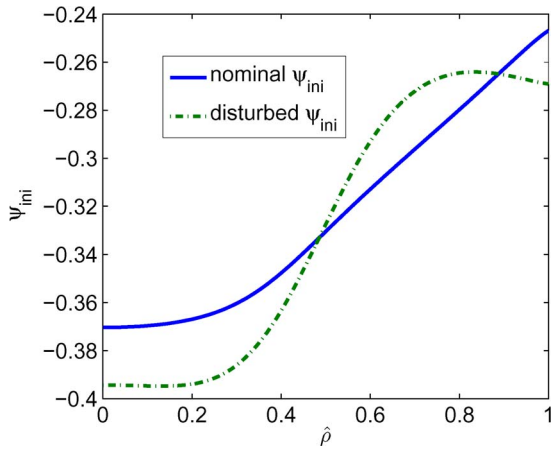

Fig. 8. Comparison of initial ψ (in webers) profiles.

In this simulation study, we choose $M_p = 1$, $A^* = 10^{-4}$, and $\omega_B^* = 10^6$ [9].

Using the derived $\Delta - P^* - K$ framework (Fig. 7), a stabilizing controller can be designed to minimize the H_∞ norm of the frequency-weighted sensitivity transfer function in the presence of resistivity (or conductivity) model uncertainties. The uncertain parameters δ_i ranges from -1 to 1, defining the range of values for the resistivity (or conductivity) for which the system should be stably controlled so that the robust controller can be considered a suitable design.

In this section, we present the simulation results showing the effectiveness of the proposed robust control algorithm in a combined reference-tracking and disturbance-rejection problem. For the simulation study, we consider the time interval $[t_0 = 0.5\,\mathrm{s}, t_f = T = 1.7\,\mathrm{s}]$, and the temperature T_e is assumed to follow $(I(t)\sqrt{P_{\mathrm{tot}}}/\bar{n}(t))$ as

$$T_e(\hat{\rho}, t) = k_{\mathrm{Te}} T_e^{\mathrm{profile}}(\hat{\rho}) \frac{I(t)\sqrt{P_{\mathrm{tot}}}}{\bar{n}(t)} \tag{46}$$

where T_e^{profile} refers to a reference profile identified from DIII-D discharges associated with the experiment of interest (shown in Fig. 2) $k_{\mathrm{Te}} = 1.7295 \cdot 10^{10}$ $(\mathrm{m}^{-3} \cdot \mathrm{A}^{-1} \cdot \mathrm{W}^{-1/2})$. This simplified model for the temperature evolution is only used for simulation purposes. Any other more complex model could be used with the same purpose since the designed controller is robust against model uncertainties in the resistivity and, therefore, in the temperature.

The nominal initial poloidal flux ψ_{ini} shown in Fig. 8 has been considered for the synthesis of an open-loop optimal controller via ES [2]. Fig. 9 shows the time evolution of the optimized open-loop actuation. Note that, from (10) and

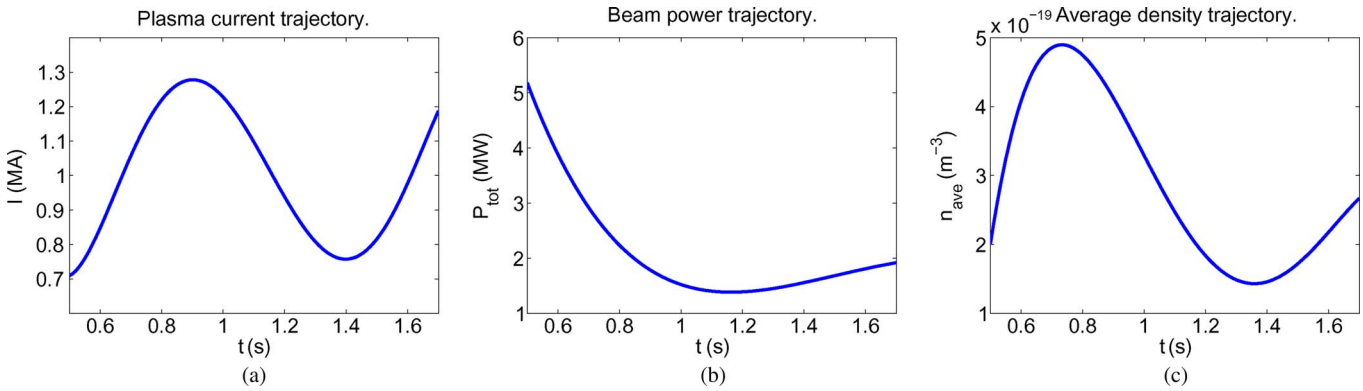

Fig. 9. Open-loop ES optimal control: (a) $I(t)$. (b) $P_{\rm tot}$. (c) $\overline{n}(t)$.

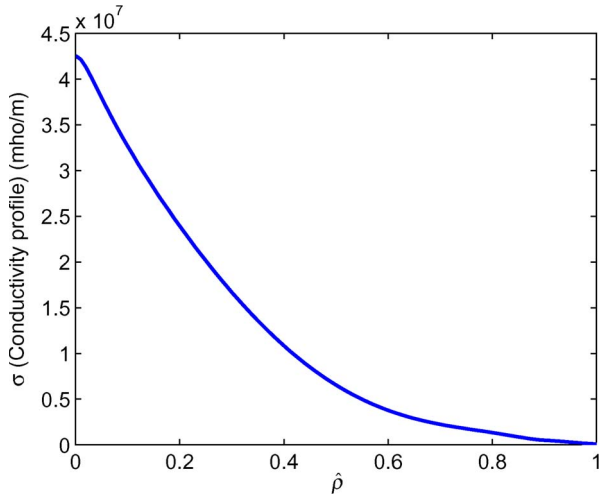

Fig. 10. Nominal conductivity profile.

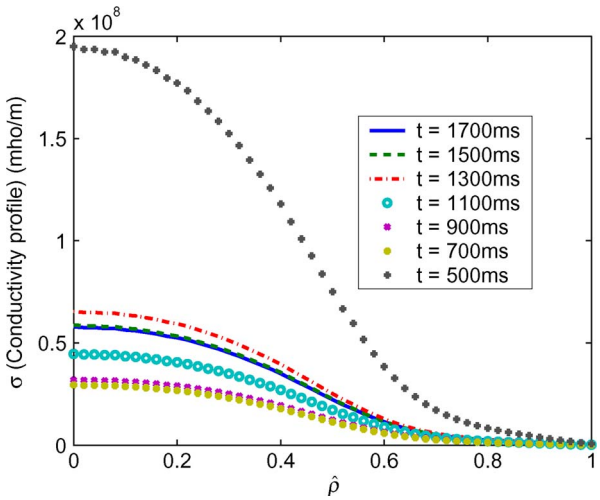

Fig. 11. Conductivity profile evolution.

(11), the control inputs are indeed functions of $I(t)$, $P_{\rm tot}(t)$, and $\overline{n}(t)$.

We consider now that the nominal initial profile used for the design of the open-loop controller is disturbed, as shown in Fig. 8. We compare the performances of both open- and closed-loop controllers in the presence of this disturbance. For the closed-loop simulation study presented in this section, we assume that the time evolution of the average density $\overline{n}(t)$ is the same as the one obtained by the open-loop ES controller. Nominal and actual conductivities σ (1/resistivity) are compared in Figs. 10–11. While Fig. 10 shows the nominal conductivity used for the synthesis of the robust H_∞ controller, Fig. 11 shows the actual evolution from 0.0 to 1.2 s as predicted by the simulation models (5) and (46). Fig. 12 compares the desired target profile ψ^d with the final-time profiles $\psi(t_f, \hat{\rho})$ obtained with both the open- and closed-loop controllers. Both final-time profiles are obtained using the disturbed initial profile in Fig. 8 when the open- and closed-loop control input trajectories are those shown in Figs. 9 and 13. The figure shows that the proposed closed-loop controller outperforms the open-loop controller by effectively tracking the nominal profile evolution when the initial condition is perturbed.

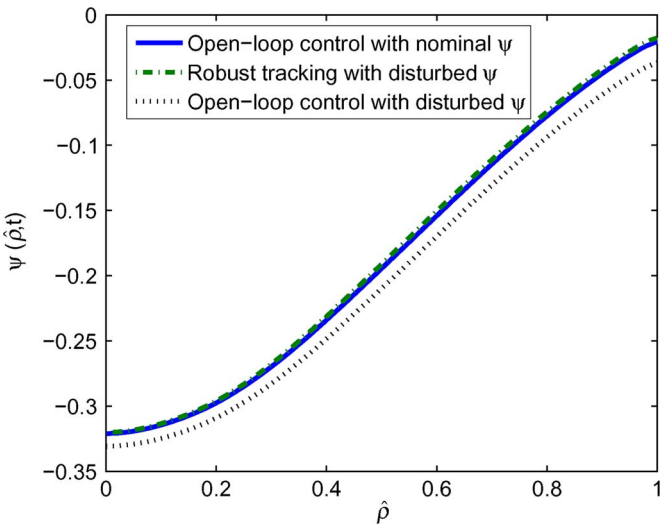

Fig. 12. Final time ψ (in webers) matching comparison.

VI. Conclusion

We consider a control-oriented dynamic model describing the evolution of the poloidal flux during the inductive phase of the tokamak discharge. Using the POD/Galerkin technique, we reformulate this partial differential equation (PDE) model into a low-dimensional ODE model that preserves the dominant dynamics of the original parabolic PDE. The resistivity term is modeled as an uncertainty, and the model is rewritten within a robust control framework $\Delta - P^* - K$. A robust closed-loop controller is synthesized to minimize the H_∞ norm of a

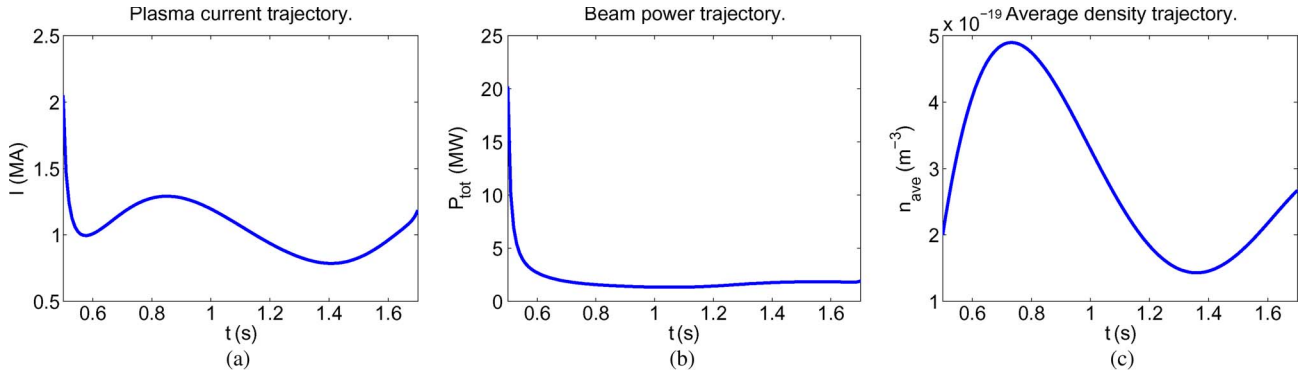

Fig. 13. Closed-loop robust tracking control: (a) $I(t)$. (b) $P_{\rm tot}$. (c) $\overline{n}(t)$.

weighted version of the sensitivity transfer function and, therefore, to minimize the weighted tracking error. The simulation study shows that the proposed robust closed-loop controller rejects the disturbance in the initial profile and improves the tracking performance when compared to the open-loop case.

REFERENCES

[1] M. Murakami, M. R. Wade, C. M. Greenfield, T. C. Luce, J. R. Ferron, H. E. St. John, J. C. Deboo, W. W. Heidbrink, Y. Luo, M. A. Makowski, T. H. Osborne, C. C. Petty, P. A. Politzer, S. L. Allen, M. E. Austin, K. H. Burrell, T. A. Casper, E. J. Doyle, A. M. Garofalo, P. Gohil, I. A. Gorelov, R. J. Groebner, A. W. Hyatt, R. J. Jayakumar, K. Kajiwara, C. E. Kessel, J. E. Kinsey, R. J. LaHaye, L. L. Lao, A. W. Leonard, J. Lohr, T. W. Petrie, R. I. Pinsker, R. Prater, T. L. Rhodes, A. C. C. Sips, G. M. Staebler, T. S. Taylor, M. A. Vanzeeland, G. Wang, W. P. West, and L. Zeng, "Progress toward fully noninductive, high beta conditions in DIII-D," *Phys. Plasmas*, vol. 13, no. 5, p. 056 106, May 2006.

[2] Y. Ou, C. Xu, E. Schuster, T. C. Luce, J. R. Ferron, M. L. Walker, and D. A. Humphreys, "Design and simulation of extremum-seeking open-loop optimal control of current profile in the DIII-D tokamak," *Plasma Phys. Control. Fusion*, vol. 50, no. 11, pp. 115 001-1–115 001-24, Sep. 2008.

[3] C. Xu, Y. Ou, J. Dalessio, E. Schuster, T. C. Luce, J. R. Ferron, M. L. Walker, and D. A. Humphreys, "Ramp-up phase current profile control of tokamak plasmas via nonlinear programming," *IEEE Trans. Plasma Sci.*, to be published.

[4] Y. Ou, E. Schuster, J. R. Ferron, T. C. Luce, M. L. Walker, D. A. Humphreys, T. A. Casper, and W. H. Meyer, "Control of the current profile evolution during the ramp-up phase at DIII-D," in *Proc. 50th Annu. Meeting Division Plasma Phys.*, Dallas, TX, 2008.

[5] K. Kunisch and S. Volkwein, "Galerkin proper orthogonal decomposition methods for parabolic problems," *Numerische Mathematik*, vol. 90, pp. 117–148, 2001.

[6] J. Wesson, *Tokamaks*, 3rd ed. Oxford, U.K.: Clarendon, 2004.

[7] Y. Ou, E. Schuster, T. Luce, J. Ferron, M. Walker, and D. Humphreys, "Towards model-based current profile control at DIII-D," *Fusion Eng. Des.*, vol. 82, no. 5–14, pp. 1153–1160, Oct. 2007.

[8] A.K. Packard, "What's new with μ: Structured uncertainty in multivariable control," Ph.D. dissertation, Univ. California, Berkeley, Berkeley, CA, 1988.

[9] K. Zhou and J.C. Doyle, *Essentials of Robust Control*. Englewood Cliffs, NJ: Prentice-Hall, 1997.

Yongsheng Ou, photograph and biography not available at the time of publication.

Chao Xu, photograph and biography not available at the time of publication.

Eugenio Schuster, photograph and biography not available at the time of publication.